Sains Malaysiana 51(4)(2022): 1229-1244
*http://doi.org/10.17576/jsm-2022-5104-22*

# The Occurred Error in Microdosimetry Calculations while Using Water Instead of the Body Organs in Proton Therapy and a New Formula for an Estimate of the Statistical Uncertainty of Microdosimetric Quantities

(Ralat Berlaku dalam Pengiraan Mikrodosimetri semasa Menggunakan Air Bukan Organ Badan dalam Terapi Proton dan Formula Baharu untuk Anggaran Ketidakpastian Statistik Kuantiti Mikrodosimetrik)

SOMAYEH JAHANFAR & HOSSEIN TAVAKOLI-ANBARAN*

*Faculty of Physics and Nuclear Engineering, Shahrood University of Technology, Shahrood, Iran*

*Received: 4 June 2021/Accepted: 26 August 2021*

ABSTRACT

In many experimental and simulation researches, water phantom is used instead of most body organs. Therefore, in this study, we replaced the water phantom instead of some organs to calculate its effect on the proton stopping-power, and range and the consequence of deposited energy and microdosimetric spectra in small sites. Some organs such as the spleen, thyroid, pancreas, prostate, testis, and ovaries are considered. We calculated the proton stopping-power in these organs using the SRIM code. Then using these results, we wrote a program in the programming language of Fortran and computed the proton range and deposited energy in two sites of 1 and 100 micron. Also, using the Geant4-10-4 code, we simulated these sites and obtained microdosimetric spectra of protons at 1 and 5MeV energies. In order to compare different states, the frequency-mean lineal energy, dose-mean lineal energy, these statistical uncertainties and absorb dose in each case were calculated and reported. Also, we estimated the statistical uncertainty of quantities with a new formula. We observed that using water instead of the organs causes a significant error in the calculations of the range and the maximum relative difference percentage of 18% and 22% in deposited energy in 1 and 100 micron sites, respectively. These differences depend on the energy of the incident proton, organ, and size site. Also, this replacement changes microdosimetric spectra, the location, and intensity of the Bragg's peak. The percent difference of location and intensity of the Bragg's peak for water instead of the spleen is -8.66 and 13.42%, respectively. Therefore, using water instead of the body organs in microdosimetry calculations is not recommended.

Keywords: Body organs and water; microdosimetry; proton range and stopping power; proton therapy; statistical uncertainty

ABSTRAK

Dalam banyak penyelidikan uji kaji dan simulasi, fantom air digunakan sebagai ganti kebanyakan organ tubuh. Oleh itu, dalam kajian ini, kami menggantikan fantom air dan bukannya beberapa organ untuk menghitung kesannya pada daya berhenti proton dan julat serta akibat daripada tenaga dan spektrum mikrodosimetri yang tersimpan di lokasi kecil. Beberapa organ seperti limpa, tiroid, pankreas, prostat, testis dan ovari dipertimbangkan. Kami menghitung daya berhenti proton pada organ-organ ini menggunakan kod SRIM. Kemudian, menggunakan hasil ini, kami menulis sebuah program dalam bahasa pengaturcaraan Fortran dan menghitung julat proton dan menyimpan tenaga di dua lokasi antara 1 dan 100 mikron. Juga, menggunakan kod Geant4-10-4, kami mensimulasi lokasi ini dan memperoleh spektrum mikrodosimetri proton pada tenaga 1 dan 5MeV. Untuk membandingkan keadaan yang berlainan, tenaga linear frekuensi-min, tenaga garis lurus-dosis, ketidakpastian statistik ini dan penyerap dos dalam setiap kes dihitung dan dilaporkan. Kami juga menganggarkan ketidaktentuan statistik kuantiti dengan formula baru. Kami memerhatikan bahawa penggunaan air sebagai ganti organ telah menyebabkan ralat yang ketara dalam pengiraan julat dan peratusan perbezaan relatif maksimum 18% dan 22% tenaga yang tersimpan masing-masing di lokasi 1 dan 100 mikron. Perbezaan ini bergantung pada tenaga proton, organ dan ukuran saiz lokasi. Juga, penggantian ini mengubah spektrum mikrodosimetri, lokasi dan keamatan puncak Bragg. Perbezaan peratus lokasi dan keamatan puncak Bragg untuk air dan bukannya limpa masing-masing adalah -8.66 dan 13.42%. Oleh itu, penggunaan air bukan organ tubuh dalam pengiraan mikrodosimetri tidak digalakkan.

Kata kunci: Julat proton dan daya berhenti; ketidaktentuan statistik; mikrodosimetri; organ badan dan air; terapi proton

## Introduction

In radiation therapy, cancer organs are exposed to ionizing radiation to prevent their growth and proliferation. To treat various cancers such as cancer of the brain, breast, lung, prostate, stomach, and other benign tumors, radiation therapy is used (Shahrabi et al. 2015). The beam emits energy along the path it travels, and so the stopping power is obtained from (1):

$$S = \frac{\kappa z_2}{\beta^2} \; Z_1^2 (L_0(\beta) + Z_1 L_1(\beta) + Z_1^2 L_2(\beta) + \ldots \;) \quad (1)$$

In this regard, L(s) are the stop numbers and include correction factors with different powers for high-velocity particles, $\beta = \upsilon / c$, $\kappa = 4\pi e^4 N / m_e c^2$, and $Z_1$ is the charge of the incident particle and $z_2$ is the atomic number of matter (Ziegler 1999; Ziegler et al. 2008). Due to the fact that the body organs are composed of different elements, so the calculation of the stopping power in the organ must include the formula of composition which is as follows:

$$(-\frac{dE}{\rho dx})_{compound} = \sum_i w_i (-\frac{dE}{\rho dx})_i \quad (2)$$

In the above relation, $\rho$ is the density and $w_i$ is the weight fraction of each element (Tsoulfanidis 2015). And the range is obtained by (3):

$$R = \int \frac{dE}{f(E)} \;, \quad (-\frac{dE}{dx}) = f(E) \quad (3)$$

Proton therapy (direct) and neutron therapy (backscattering of the nucleus of hydrogen atoms) require accurate information on the mechanism of energy transfer of protons to the organ (Khan et al. 2014). Therefore, according to the different sensitivities of the organs to radiation in order to calculate the deposited energy in the organ (Rasouli et al. 2017), gathering accurate information about the stopping power and consequently the range of the beam in different organs is important. On the other hand, due to the easy access and homogeneity of water and the proximity of water absorption properties to soft tissues (Liu et al. 2003) as well as the proximity of water density to body organs, this substance has become an important substance in biology and in most researches, the water is used instead of body organs (Akiyama et al. 1992; Blosser et al. 1964; Thomas et al. 1979; Toburen et al. 1977).

According to Mitchell et al. (1945), the chemical composition of different organs is different and therefore the share of water in them is also different. In adults, for example, the brain, heart, pancreas, lungs, kidneys, spleen, liver, and skin are made up of 73.33, 73.69, 73.08, 83.74, 79.47, 78.69, 71.46, and 64.68% water, respectively, and even the bones are made up of 31.81% water (Mitchell et al. 1945). Also, because the human body is made up of different organs with different densities, using water instead of the real organ can be one of the sources of error (Ahmadi & Tavakoli-Anbaran 2015) to determine the stopping power and range and consequently deposited energy in tissue accurately. In the following, it is necessary to briefly state the quantities used in microdosimetry. Lineal energy ( $y = \frac{\varepsilon_1}{\bar{l}}$) is expressed as $\frac{keV}{\mu m}$ and $\bar{l}$ is the mean chord length, and $\varepsilon_1$ is the energy imparted in the target in a single event (Cornelius et al. 2002; Lindborg et al. 2017; Northum et al. 2012; Reniers et al. 2004; Rosenfeld et al. 2000; Tsuda et al. 2010). Cauchy's theorem for a convex object states: The mean chord length is $4V/S$, where V and S are the volume and surface of the site, respectively. Lineal energy distribution f(y) is the probability density of lineal energy and f(y)dy is the probability of lineal energy being in the event of an interval of $[y, y+dy]$ (Bolst et al. 2017; Rossi et al. 2011). The dose probability density is defined as follow:

$$d(y) = \frac{y}{\bar{y}_F} \; f(y) \quad (4)$$

In the above relation, $\bar{y}_F$ is known as the frequency-mean lineal energy, as follows (Burigo et al. 2013; ICRU 1983; Kliauga & Rossi 1982; Rosenfeld 2016).

$$\bar{y}_F = \int_0^\infty y f(y) dy \quad (5)$$

Also, the dose-mean lineal energy defines as follows (Chattaraj et al. 2018; Pan et al. 2015).

$$\bar{y}_D = \int_0^\infty y d(y) dy = \frac{\int_0^\infty y^2 f(y) dy}{\int_0^\infty y f(y) dy} \quad (6)$$

The statistical uncertainty estimated in $\bar{y}_F$ using the error propagation formula is given as:

$$\frac{\sigma_{\bar{y}_F}}{\bar{y}_F} = \sqrt{\frac{\sum_i y_i^2 f(y_i)}{(\sum_i y_i f(y_i))^2} + \frac{\sum_i f(y_i)}{(\sum_i f(y_i))^2}} \quad (7)$$

A similar expression results for $\overline{y}_D$ (Aslam et al. 2003). In this article, we examined what errors and changes that occur in the calculations of stopping power and range and consequently, the deposited energy in the site and also in microdosimetric spectra through placing water instead of some organs in proton therapy. We also estimated the statistical uncertainty of quantities with a new formula and compared these quantities in different states with two formulas.

## Materials and Methods

In this article, using the SRIM code, we obtained the proton stopping power in liquid water and six organs of the body's important organs, including the spleen, thyroid, pancreas, prostate, testicles, and ovaries, the elements of each are stated in Table 1.

Since the stopping power is a complicated expression, a numerical integration is required. In order to calculate the range and deposited energy, we wrote a program in the Fortran programming language using formula 3, the proton stopping power data of the SRIM code for water and the mentioned organs and dimension site. Formula 3 is divided into $N$ segments of $\Delta E_i$, $R = \sum_i^N \frac{\Delta E_i}{-(dE/dx)_i}$, where $(dE/dx)_i$ is the stopping power calculated for the kinetic energy of the particle at the beginning of the segment $\Delta E_i$.

TABLE 1. Elements and weight fractions of some organs of the body (Ziegler et al. 2008)

| Spleen | | Testis | | Thyroid | |
|---|---|---|---|---|---|
| Elements | weight fractions | Elements | weight fractions | Elements | weight fractions |
| H | 10.31 | H | 10.61 | H | 10.42 |
| C | 11.31 | C | 9.91 | C | 11.92 |
| N | 3.20 | N | 2.00 | N | 2.40 |
| O | 74.17 | O | 76.68 | O | 74.65 |
| P | 0.30 | Na | 0.20 | Na | 0.20 |
| S | 0.20 | S | 0.20 | Cl | 0.20 |
| Cl | 0.20 | Cl | 0.20 | K | 0.10 |
| K | 0.30 | K | 0.20 | I | 0.10 |
| Ovary | | Pancreas | | Prostate | |
| Elements | weight fractions | Elements | weight fractions | Elements | weight fractions |
| H | 10.52 | H | 10.62 | H | 10.50 |
| C | 9.32 | C | 16.93 | C | 8.90 |
| N | 2.40 | N | 2.20 | N | 2.50 |
| O | 76.95 | O | 69.54 | O | 77.40 |
| P | 0.20 | P | 0.20 | Na | 0.20 |
| S | 0.20 | S | 0.10 | P | 0.10 |
| Cl | 0.20 | Cl | 0.20 | S | 0.20 |
| K | 0.20 | K | 0.20 | K | 0.20 |

Then to verify our program, we wrote an input file using the MCNPX code for the proton point source at 200 MeV. We placed a sphere of the water in front of the source. In this code, we obtained the stopping power of the proton using the print card and output table 85. We compared results of the proton range of our own program in Fortran with the results obtained from the MCNPX code, and after ensuring the performance of our program, we calculated the range and deposited energy in the 1 and 100 micron sites using this program. We also calculated the relative difference of proton range in water and each of these organs. In addition, we calculated and plotted the Bragg peak curve in terms of different thicknesses of water and organs. In the following, using the Geant4-10-4 code, we simulated sites of 1 and 100 microns of water and body organs for the proton with energies of 1 and 5 MeV and 0 micron cut-off.

Micron sites with water materials and organs were simulated in the detector-construction class and physics were also simulated using reference physics lists of QGSP_BIC_HP in the physics-list class. We considered the 300 logarithmic intervals of lineal energy from 0.001 to 1000$\frac{keV}{\mu m}$ and 50 logarithmic intervals per decade, the probability density of lineal energy or f(y) in each interval is calculated so that finally we calculated the microdosimetric spectra using formulas 4 and 5. We also used formulas 5, 6, and 7 to calculate other microdosimetric quantities and statistical uncertainty of these quantities. It is worth noting that the information required for Monte Carlo simulations according to Sechopoulos et al. (2018) is stated.

We also estimated the statistical uncertainty of quantities with a new formula. Assume that in arbitrary function f(x), the quantity x is examined. In the problems studied by the Monte Carlo method, $f(x_i)$ is counts or frequency of quantity x in the bin "i", N is the total number of bins, $f(x_i) = n_i/\Delta y_i$, standard deviation of Poisson distribution function $\sigma_{f(x_i)} = \sqrt{n_i}/\Delta y_i$ and $G(x) = x^b f(x)$. If the lineal energy widths of the intervals are the same $\sigma_{f(x_i)} = \sqrt{n_i}/\Delta y$. The average or the expectation value of x, is defined by the equation:

$$\langle \mathrm{x} \rangle = \bar{\mathrm{x}} = \frac{\int_0^\infty \mathrm{xG(x)dx}}{\int_0^\infty \mathrm{G(x)dx}} = \frac{\sum_{\mathrm{i=1}}^{\mathrm{N}} \mathrm{x_i x_i{}^b f(x_i)}}{\sum_{\mathrm{i=1}}^{\mathrm{N}} \mathrm{x_i{}^b f(x_i)}} = \frac{\sum_{\mathrm{i=1}}^{\mathrm{N}} \mathrm{x_i{}^{b+1} n_i}}{\sum_{\mathrm{i=1}}^{\mathrm{N}} \mathrm{x_i{}^b n_i}} = \frac{\mathrm{S_b}}{\mathrm{M_b}} \quad (8)$$

we have from the error propagation formula:

$$\sigma_{\bar{x}}^2 = \left(\frac{\partial \bar{x}}{\partial f_1}\sigma_{f_1}\right)^2 + \cdots + \left(\frac{\partial \bar{x}}{\partial f_i}\sigma_{f_i}\right)^2 + \cdots = \sum \left(\frac{\partial \bar{x}}{\partial f_i}\sigma_{f_i}\right)^2$$

$$\sigma_{\bar{x}}^2 = \sum_{i=1}^{N}\left(\frac{x_i{}^{b+1}M_b - x_i{}^b S_b}{M_b{}^2}\sigma_{f_i}\right)^2 = \sum_{i=1}^{N}\frac{\left(x_i{}^{2b+2}M_b{}^2 - 2x_i{}^{2b+1}M_b S_b + x_i{}^{2b}S_b{}^2\right)}{M_b{}^4}\sigma_{f_i}^2 = \quad (9)$$

$$\frac{1}{(\Delta y)^2}\left(\frac{\sum_{i=1}^{N} x_i{}^{2b+2}M_b{}^2 n_i}{M_b{}^4} - \frac{\sum_{i=1}^{N} 2\, x_i{}^{2b+1}M_b S_b n_i}{M_b{}^4} + \frac{\sum_{i=1}^{N} x_i{}^{2b}S_b{}^2 n_i}{M_b{}^4}\right)$$

We will have:

$$\sigma_{\bar{x}}^2 = \frac{1}{(\Delta y)^2}\left(\frac{\sum_{i=1}^{N} x_i{}^{2b+2} n_i}{M_b{}^2} - \frac{2\, S_b \sum_{i=1}^{N} x_i{}^{2b+1} n_i}{M_b{}^3} + \frac{S_b{}^2 \sum_{i=1}^{N} x_i{}^{2b} n_i}{M_b{}^4}\right) \quad (10)$$

We rewrite (10) by $f(x_i) = n_i/\Delta y$:

$$\sigma_{\bar{x}}^2 = \frac{1}{\Delta y}\left(\frac{\sum_{i=1}^{N} x_i{}^{2b+2} f(x_i)}{M_b{}^2} - \frac{2\, S_b \sum_{i=1}^{N} x_i{}^{2b+1} f(x_i)}{M_b{}^3} + \frac{S_b{}^2 \sum_{i=1}^{N} x_i{}^{2b} f(x_i)}{M_b{}^4}\right) \quad (11)$$

By replacing $x_i$ to $y_i$ we have:

$$\sigma_{\bar{x}}^2 = \frac{1}{\Delta y}\left(\frac{\sum_{i=1}^{N} y_i{}^{2b+2} f(y_i)}{M_b{}^2} - \frac{2\, S_b \sum_{i=1}^{N} y_i{}^{2b+1} f(y_i)}{M_b{}^3} + \frac{S_b{}^2 \sum_{i=1}^{N} y_i{}^{2b} f(y_i)}{M_b{}^4}\right) \quad (12)$$

If b = 0 then $\frac{\sum_{i=1}^{N} y_i f(y_i)}{\sum_{i=1}^{N} f(y_i)} = \frac{S_0}{M_0}$ and the statistical uncertainty of $\bar{y}_F$ will be as follows

$$\sigma_{\bar{y}_F}^2 = \frac{1}{\Delta y}\left(\frac{\sum_{i=1}^{N} y_i{}^2 f(y_i)}{M_0{}^2} - \frac{2\, S_0 \sum_{i=1}^{N} y_i f(y_i)}{M_0{}^3} + \frac{S_0{}^2 \sum_{i=1}^{N} f(y_i)}{M_0{}^4}\right) \quad (13)$$

Finally, (14) is obtained:

$$\sigma_{\bar{y}_F}^2 = \frac{1}{\Delta y}\left(\frac{\sum_{i=1}^{N} y_i{}^2 f(y_i)}{M_0{}^2} - \frac{2\, S_0{}^2}{M_0{}^3} + \frac{S_0{}^2}{M_0{}^3}\right) = \frac{1}{\Delta y}\left(\frac{\sum_{i=1}^{N} y_i{}^2 f(y_i)}{M_0{}^2} - \frac{S_0{}^2}{M_0{}^3}\right)$$

$$\sigma_{\bar{y}_F}^2 = \frac{1}{\Delta y}\left(\frac{\sum_{i=1}^{N} y_i{}^2 f(y_i)}{(\sum_{i=1}^{N} f(y_i))^2} - \frac{(\sum_{i=1}^{N} y_i f(y_i))^2}{(\sum_{i=1}^{N} f(y_i))^3}\right) \quad (14)$$

If b = 1 then $\frac{\sum_{i=1}^{N} y_i{}^2 f(y_i)}{\sum_{i=1}^{N} y_i f(y_i)} = \frac{S_1}{M_1}$ and the statistical uncertainty of $\bar{y}_D$ will be as follows:

$$\sigma_{\bar{y}_D}^2 = \frac{1}{\Delta y}\left(\frac{\sum_{i=1}^{N} y_i{}^4 f(y_i)}{M_1{}^2} - \frac{2\, S_1 \sum_{i=1}^{N} y_i{}^3 f(y_i)}{M_1{}^3} + \frac{S_1{}^2 \sum_{i=1}^{N} y_i{}^2 f(y_i)}{M_1{}^4}\right) \quad (15)$$

And finally, (16) is obtained:

$$\sigma_{\overline{y_D}}^2 = \frac{1}{\Delta y}\left(\frac{\sum_{i=1}^{N} y_i^4 f(y_i)}{{M_1}^2} - \frac{2\,S_1 \sum_{i=1}^{N} y_i{}^3 f(y_i)}{{M_1}^3} + \frac{{S_1}^3}{{M_1}^4}\right) \quad (16)$$

$$\sigma_{\overline{y_D}}^2 = \frac{1}{\Delta y}\left(\frac{\sum_{i=1}^{N} y_i^4 f(y_i)}{(\sum_{i=1}^{N} y_i f(y_i))^2} - \frac{2\,\sum y_i^2 f(y_i) \sum_{i=1}^{N} y_i^3 f(y_i)}{(\sum_{i=1}^{N} y_i f(y_i))^3} + \frac{(\sum_{i=1}^{N} y_i^2 f(y_i))^3}{(\sum_{i=1}^{N} y_i f(y_i))^4}\right)$$

In order to compare different states, the frequency-mean lineal energy, dose-mean lineal energy, and these statistical uncertainties with the formulas 7, 14, and 16 and absorb dose in each case were calculated and reported, which its results are described in the next section.

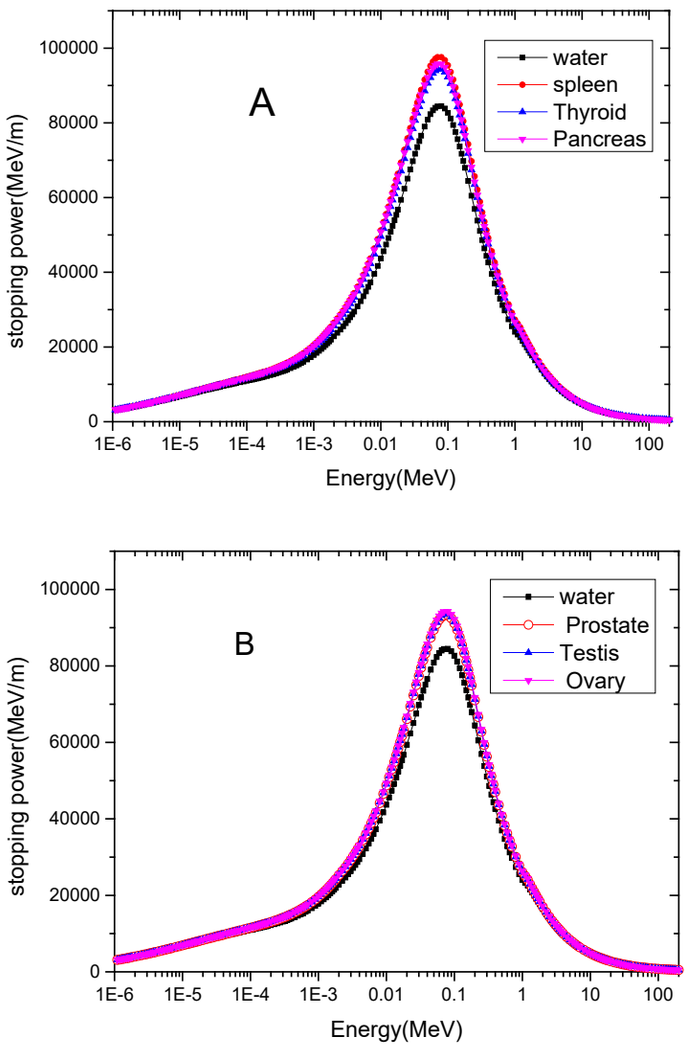


FIGURE 1. Stopping power curve versus proton energy in water (black curve) in comparison with organs of (a) spleen (red curve), thyroid (blue curve) and pancreas (purple curve) (b) prostate (red curve), testis (blue curve), and ovary (purple curve)

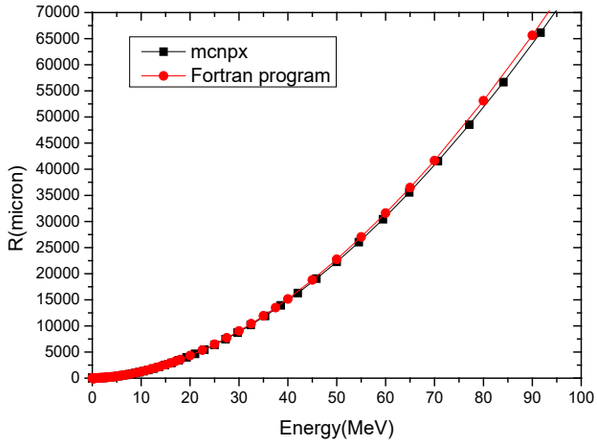


FIGURE 2. Calculation of the proton range in water. The black curve through the MCNPX code and the red curve through our code

## RESULTS AND DISCUSSION

The proton stopping power curves in terms of energy in water, spleen, thyroid, and pancreas prostate, testicles, and ovaries are plotted in Figure 1(a) and 1(b). Using Figure 1, it can be seen that the proton stopping power curves in water and in these organs are different.

In order to verify the above program, we calculated the proton range in water through the MCNPX code,

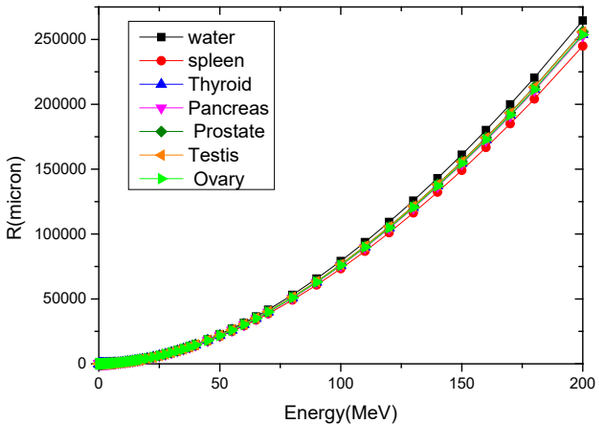


FIGURE 3. Proton range curve up to the energy of 200 MeV in terms of the energy in water (black curve) in comparison with the spleen (red), thyroid (light blue), pancreas (pink), prostate (dark green), testis (Orange), and ovary (light green)

and the results of our code and MCNPX code are plotted in Figure 2. This figure shows good agreement between the two codes.

Then, we calculated the proton range by using our code in all of the above-mentioned organs. The proton range is plotted up to 200 MeV energy in Figure 3.

In macro sites, the proton range in water can be considered equivalent to these organs with a good approximation. However, when the dimensions of the site become small and turns to micro order, due to the difference in the stopping power and range, the difference between water and these organs is considerable. For

example, for a proton with 10 MeV energy; the range value in water is 1.25 mm, While the range values in spleen and thyroid are 1.16 and 1.20 mm, respectively. To examine Figure 3 more closely, we drew Figure 4 for protons with energies of 1.2 to 1.4 MeV. According to this figure, it is observed that among the mentioned organs, the spleen has the lowest range and the prostate has the highest range. Assuming that the proton moves in a straight line, according to Figure 4, a proton with 1.3 MeV energy in the 36 micron site of the spleen and this proton in the 37.6 micron site of the prostate deposits all its energy in the site. Therefore, this proton will stop in the site of 36 to 38 microns in the mentioned organs. But if the same proton moves in water, it deposits all its energy in a site of approximately 40.9 micron. Therefore, in the 38 micron site and at 1.3 MeV energy, if we use

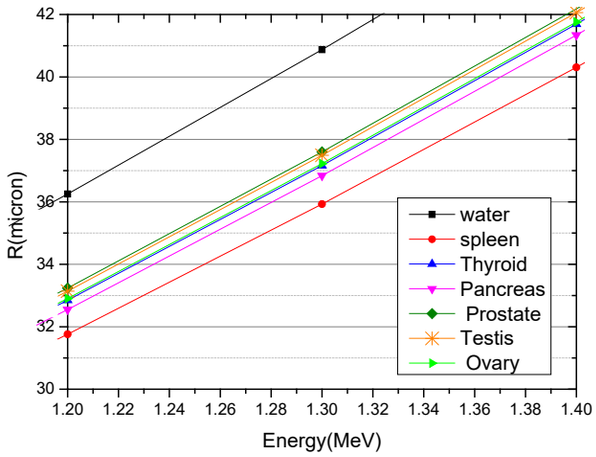


FIGURE 4. Proton range curve in terms of energies of 1.2 to 1.4 MeV in water (black curve) in comparison with the spleen (red), thyroid (light blue), pancreas (pink), prostate (green Dark), testis (orange), and ovary (light green)

water instead of the mentioned organs, this proton will leave the mentioned site at the end of the path and as a result, part of its energy will be transferred out of the site.

The radiation used in radiation therapy should be such that in spite of covering the complete tumor during therapy, the possibility of reaching the surrounding healthy tissues and organs is minimized (Rasouli et al. 2018). Therefore, as stated above, assuming that the tumor is placed inside the site, the beam exits from the site and damages nearby healthy tissues and organs, and especially when the tumor site is located near a vital organ in the body, it will damage this healthy organ.

Also, in order to study and compare the difference between the proton range in water and organs, in Table 2, we showed the proton range in terms of the incident proton with different energies in the water and organs. According to this table, protons with higher energies gets the larger range. The higher the proton energy is, the higher the proton velocity; and the proton has less opportunity to interact with matter, so the probability of a collision is reduced and the range is increased.

It is also observed that at low energies the difference of proton range in water will increase compared to different organs, and with increasing energy of the incident proton the difference of proton range in water and organs will be less. Since accurate calculation of the proton range is very important in microdosimetry, the use of water instead of the organ will cause a significant error in microdosimetric calculations, especially at low energies.

Then, in order to clarify the difference between water and body organs in microdosimetric calculations, we calculated the percent of the relative difference of the proton range in water in comparison with each of the mentioned organs. The results of these relative differences percentage of these organs are plotted in Figure 5.

Figure 6(a) and 6(b) are also drawn to compare the relative difference of proton range in water with all the organs mentioned in this study. This figure shows that the relative difference of proton range in water is highest for the spleen and lowest for the prostate.

TABLE 2. Range (μm) of incident protons in different organs in terms of energy (keV)

| Energy(keV) | Water | Pancreas | Thyroid | Spleen |
|---|---|---|---|---|
| 0.01 | 0.00203 | 0.00194 | 0.00197 | 0.00192 |
| 0.1 | 0.01142 | 0.01068 | 0.01089 | 0.01058 |
| 1 | 0.07232 | 0.06493 | 0.0663 | 0.06432 |
| 10 | 0.35639 | 0.31023 | 0.31754 | 0.30771 |
| 100 | 1.55582 | 1.36066 | 1.38631 | 1.3418 |
| 1000 | 27.53493 | 24.56201 | 24.80258 | 23.98274 |
| 10000 | 1252.505 | 1193.184 | 1198.311 | 1157.476 |
| 50000 | 22759.14 | 21735.98 | 21814.84 | 21064.03 |
| 100000 | 79199.4 | 75668.49 | 75925.34 | 73301.24 |
| 200000 | 264553.6 | 252842.6 | 253653.1 | 244862.3 |
| Energy(keV) | Water | Ovary | Testis | Prostate |
| 0.01 | 0.00203 | 0.00197 | 0.00198 | 0.00199 |
| 0.10 | 0.01142 | 0.01089 | 0.01093 | 0.01101 |
| 1.00 | 0.07232 | 0.0665 | 0.06678 | 0.06725 |
| 10.00 | 0.35639 | 0.31907 | 0.32052 | 0.32275 |
| 100.00 | 1.55582 | 1.39066 | 1.39841 | 1.40622 |
| 1000.00 | 27.53493 | 24.84974 | 25.02623 | 25.10336 |
| 10000.00 | 1252.505 | 1198.451 | 1208.183 | 1210.351 |
| 50000.00 | 22759.14 | 21814.57 | 21993.54 | 22026.35 |
| 100000.00 | 79199.4 | 75909.14 | 76545.32 | 76649.98 |
| 200000.00 | 264553.6 | 253577.7 | 255720.1 | 256074.8 |

However, for example, at 10 MeV energy the relative error percentage of the proton range for the spleen is 8.69% and for the prostate is 3.95%. It is also observed that at high energy protons this relative error percentage is constant, and as we move towards the incident protons with energies less than 10 MeV, this relative error percentage with a relatively steeper slope will be higher.

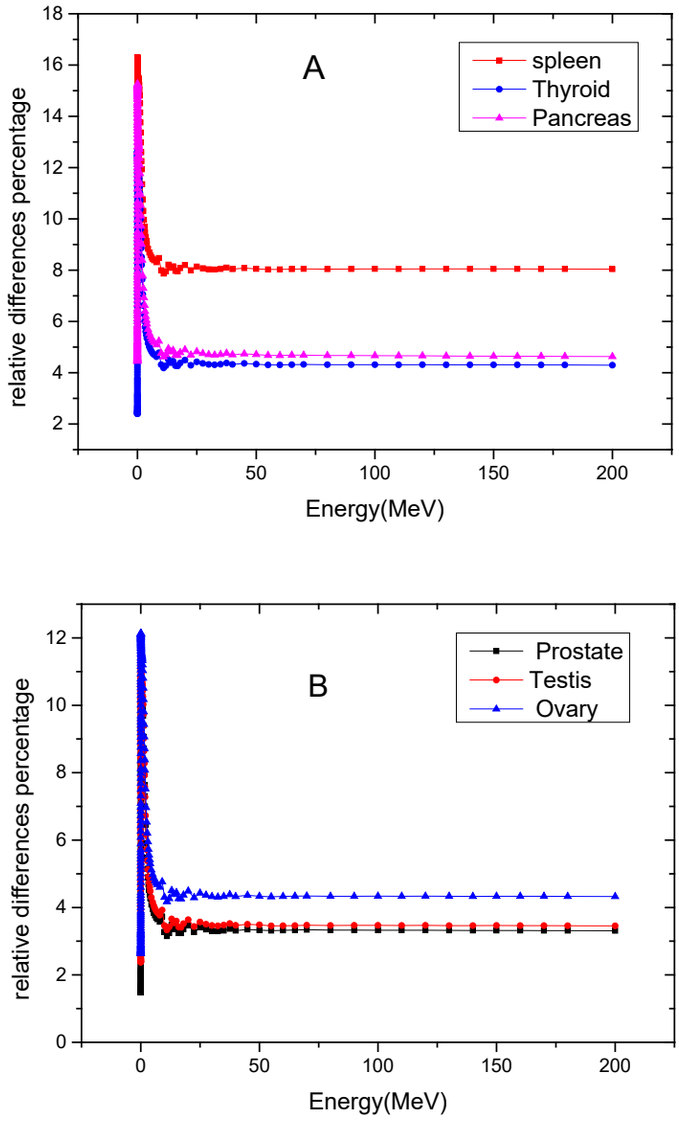


FIGURE 5. Percent of the relative difference of proton range up to 200 MeV energy in water in comparison with each of the organs a) spleen (red), thyroid (blue), pancreas (purple) b) prostate (black), testis (red), Ovary (blue)

Then, with our code, we calculated the deposited energy of the protons in water and these organs in the sites of one and 100 microns. In Table 3, according to the energy of the incident proton at the site of one micron and 100 micron, the deposited energy of the proton (in terms of keV) in water in comparison with the organs is expressed.

In the 1 micron site, the difference of deposited energy for low-energy protons in organs and water on microdosimetry cannot be ignored and must be carefully calculated.

As can be deduced from this table in the 100 micron site at low energies the difference of the deposited

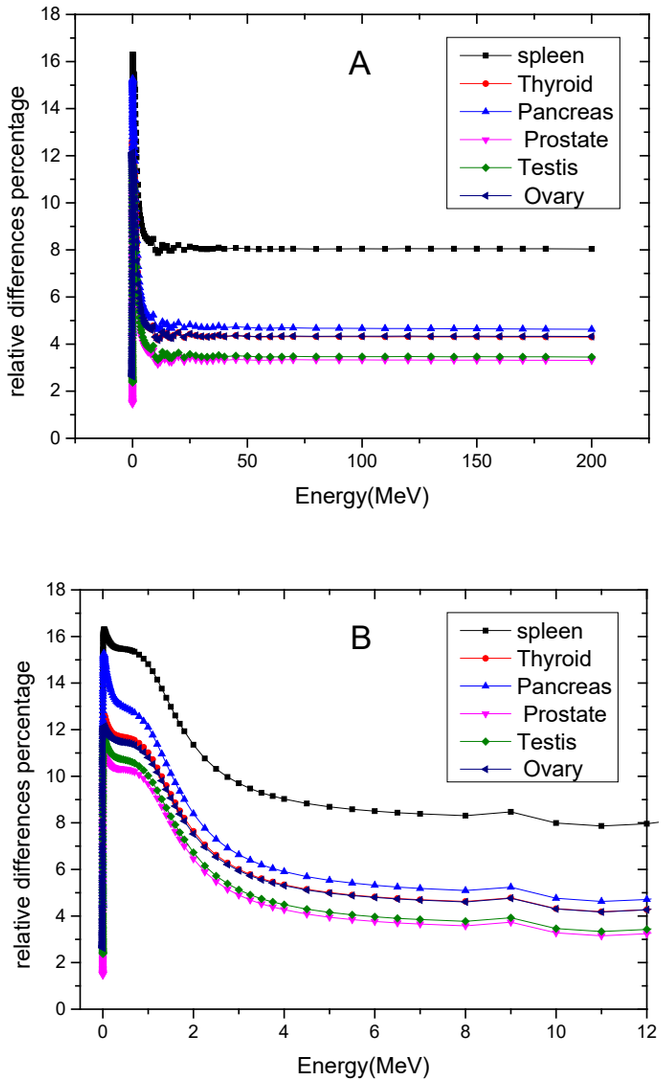


FIGURE 6. Percentage of the relative difference of proton range (a) up to 200 MeV energy and (b) up to 12 MeV energy in each of the organs of the spleen (black), thyroid (red), pancreas (light blue), prostate (purple) testis (green), Ovary (dark blue)

energy of protons in water and organs is different, but as the proton energy increases, this amount decreases rapidly. Also, in the 1 micron site for protons at 150 keV energy, the deposited energy in the spleen is 12.75 keV higher than water, and in the site of 100 micron for protons at 2.5 MeV energy, this difference is 415.3 keV, which difference of the deposited energy of protons in water compared to organs is significant.

Figure 7 shows the stopping power in terms of thickness in the water and the mentioned organs for protons with two energies of 5 and 1 MeV. One can see in this figure that the position and height of the Bragg's peak in water and tissues are different.

Since in a therapeutic process which depends on the type and depth of the tumor or cancerous tissue, the energy of the beam should be selected in such a way that the Bragg's peak is located in the site position of the tumor, and the tumor receives maximum energy and healthy surrounding tissues minimizes damage.

Therefore, in proton therapy, considering water phantom instead of tissue does not cause deposit maximum energy in the tumor site (Jahanfar & Tavakoli-Anbaran 2019) and therefore in small dimensions, the use of water phantom instead of these organs is not recommended.

The percent difference between the position and intensity of the water Bragg's peak compared to the above organs is shown in Table 4. This table makes clear that the most differences are related to the spleen tissue.

TABLE 3. Deposited energy of the incident proton (keV) in terms of energy in the 1 micron site and in the 100 micron site in different organs

| Energy (keV) | 1 Micron Site | | | | | | |
|---|---|---|---|---|---|---|---|
| | Water | Ovary | Testis | Prostate | Pancreas | Thyroid | Spleen |
| 150 | 80.00 | 89.39 | 88.85 | 88.57 | 90.85 | 88.92 | 92.75 |
| 500 | 37.04 | 40.98 | 40.98 | 40.65 | 41.67 | 41.32 | 42.74 |
| 1000 | 24.39 | 27.03 | 26.32 | 26.32 | 26.32 | 26.32 | 27.03 |
| 5000 | 8.06 | 8.47 | 8.33 | 8.33 | 8.47 | 8.47 | 8.77 |
| 10000 | 4.76 | 4.83 | 4.76 | 4.76 | 4.95 | 4.83 | 4.98 |
| 50000 | 1.25 | 1.32 | 1.32 | 1.32 | 1.32 | 1.32 | 1.35 |
| 100000 | 0.73 | 0.77 | 0.76 | 0.76 | 0.77 | 0.77 | 0.80 |
| 200000 | 0.44 | 0.46 | 0.46 | 0.46 | 0.47 | 0.46 | 0.49 |
| Energy (keV) | 100 Micron Site | | | | | | |
| | Water | Ovary | Testis | Prostate | Pancreas | Thyroid | Spleen |
| 2500 | 1853.1 | 2066.4 | 2026.2 | 2027.6 | 2107.2 | 2065.8 | 2268.4 |
| 3500 | 1206.0 | 1275.2 | 1253.1 | 1257.8 | 1280.1 | 1273.6 | 1323.1 |
| 5000 | 833.3 | 879.6 | 870.4 | 863.6 | 879.6 | 879.6 | 913.5 |
| 7000 | 625.0 | 657.5 | 650.7 | 650.7 | 659.7 | 657.5 | 685.7 |
| 10000 | 476.19 | 483.09 | 476.19 | 476.19 | 495.05 | 483.09 | 497.51 |
| 30000 | 190.84 | 198.41 | 196.85 | 196.85 | 200.00 | 198.41 | 204.92 |
| 50000 | 125.00 | 131.58 | 131.58 | 131.58 | 131.58 | 131.58 | 135.14 |
| 70000 | 96.15 | 102.04 | 100.00 | 100.00 | 102.04 | 102.04 | 104.16 |
| 100000 | 73.53 | 76.92 | 76.33 | 76.33 | 76.92 | 76.92 | 80.00 |
| 200000 | 44.45 | 46.51 | 46.51 | 46.51 | 47.62 | 46.51 | 48.78 |

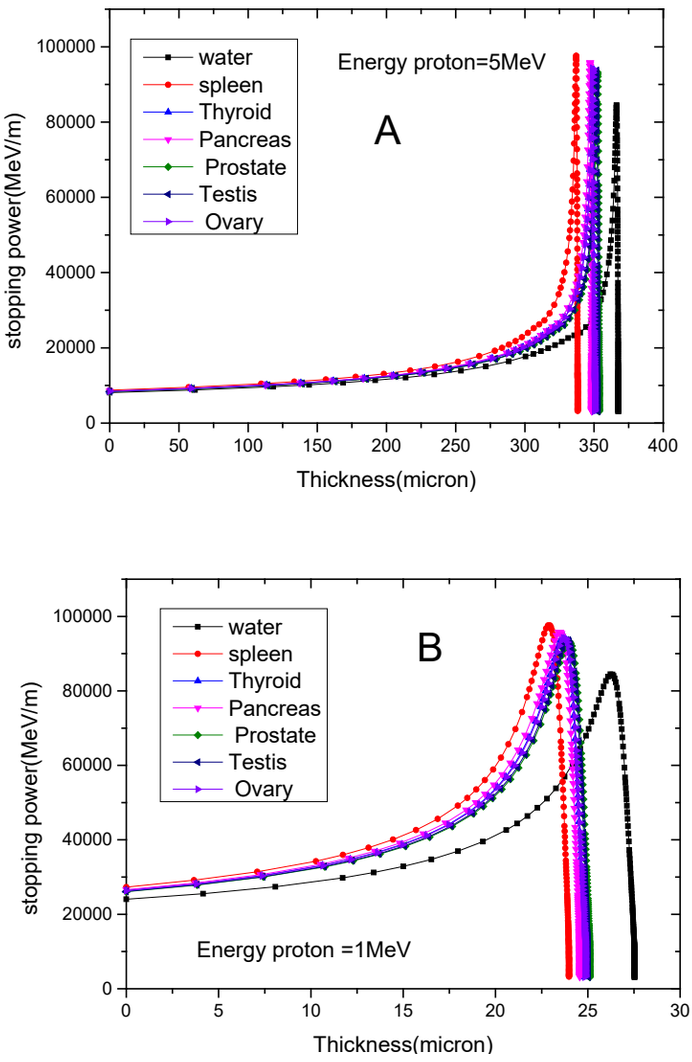


FIGURE 7. Stopping power in terms of thickness in water and body organs for protons with a) 5 MeV and b) 1 MeV energy

TABLE 4. Percent difference of position and intensity of water Bragg's peak compared to some organs

| Organ | Percent difference of position of water Bragg's peak compared to some organs | Percent difference of intensity of water Bragg's peak compared to some organs |
|---|---|---|
| Spleen | -8.66 | 13.42 |
| Thyroid | -4.98 | 10.50 |
| Pancreas | -5.47 | 11.80 |
| Prostate | -3.92 | 9.37 |
| Testis | -4.13 | 9.77 |
| Ovary | -4.96 | 10.33 |

In the following, we simulated microdosimetric spectra by using geant4-10-4 code. The results of our simulation in 1 micron site for protons at 1 MeV energy in water and organs plotted in Figure 8(a) and in 100 micron site at 5 MeV energy showed in Figure 8(b). Table 5 also reports the calculated values of frequency-mean lineal energy, dose-mean lineal energy, and these statistical uncertainties were obtained in each case by using formulas 14, 16, and 7.

Using Figure 8 and Table 5, we observed that the replacement of water instead of the body organs changes the microdosimetric spectra, frequency-mean lineal energy, dose-mean lineal.

TABLE 5. values of frequency-mean lineal energy, dose-mean lineal energy, and these statistical uncertainties in 1 micron site at 1 MeV energy and in 100 micron site at 5 MeV energy for protons in water and organs. Respectively *, ** and *** obtained using formulas 14,16 and 7

| Organ/Water | Proton point source 1 MeV in site 1 micron | | | | | |
|---|---|---|---|---|---|---|
| | $\bar{y}_f\left[\frac{keV}{\mu m}\right]$ | $\frac{\partial_{\bar{y}_f}}{\bar{y}_f}\%*$ | $\frac{\partial_{\bar{y}_f}}{\bar{y}_f}\%***$ | $\bar{y}_d\left[\frac{keV}{\mu m}\right]$ | $\frac{\partial_{\bar{y}_d}}{\bar{y}_d}\%**$ | $\frac{\partial_{\bar{y}_d}}{\bar{y}_d}\%***$ |
| Spleen | 43.410 | 0.209 | 1.988 | 44.379 | 0.211 | 2.011 |
| Prostate | 41.495 | 0.209 | 1.943 | 42.465 | 0.210 | 1.966 |
| Pancreas | 42.183 | 0.210 | 1.959 | 43.155 | 0.211 | 1.982 |
| Ovary | 41.905 | 0.209 | 1.953 | 42.878 | 0.211 | 1.976 |
| Testis | 41.585 | 0.209 | 1.945 | 42.556 | 0.211 | 1.968 |
| Water | 40.162 | 0.210 | 1.911 | 41.139 | 0.211 | 1.935 |
| Thyroid | 41.905 | 0.209 | 1.953 | 42.874 | 0.211 | 1.976 |
| Organ/Water | Proton point source 5 MeV in site 100 micron | | | | | |
| | $\bar{y}_f\left[\frac{keV}{\mu m}\right]$ | $\frac{\partial_{\bar{y}_f}}{\bar{y}_f}\%*$ | $\frac{\partial_{\bar{y}_f}}{\bar{y}_f}\%***$ | $\bar{y}_d\left[\frac{keV}{\mu m}\right]$ | $\frac{\partial_{\bar{y}_d}}{\bar{y}_d}\%**$ | $\frac{\partial_{\bar{y}_d}}{\bar{y}_d}\%***$ |
| Spleen | 14.120 | 0.036 | 1.139 | 14.146 | 0.053 | 1.141 |
| Prostate | 13.435 | 0.036 | 1.112 | 13.471 | 0.052 | 1.113 |
| Pancreas | 13.650 | 0.036 | 1.121 | 13.696 | 0.053 | 1.122 |
| Ovary | 13.579 | 0.036 | 1.118 | 13.614 | 0.052 | 1.119 |
| Testis | 13.462 | 0.036 | 1.113 | 13.498 | 0.053 | 1.114 |
| Water | 12.955 | 0.035 | 1.092 | 12.990 | 0.052 | 1.093 |
| Thyroid | 13.577 | 0.036 | 1.118 | 13.613 | 0.053 | 1.119 |

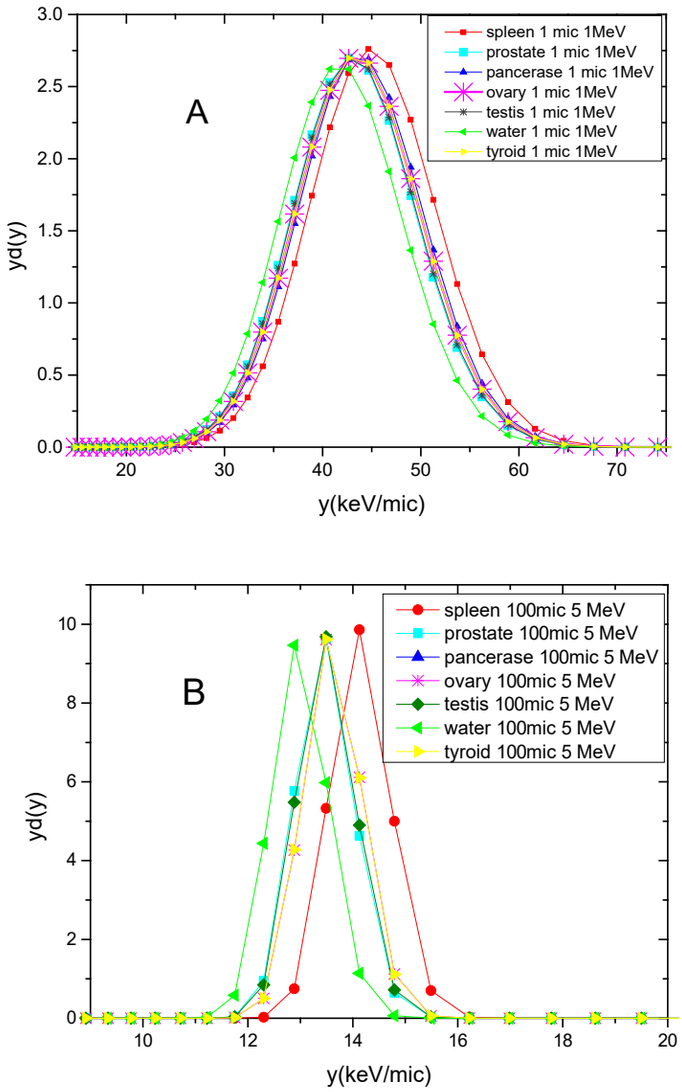


FIGURE 8. Microdosimetric spectra for protons in water and organs (a) at 1 MeV energy in 1 micron site (b) at 5 MeV energy in 100 micron site

Also, according to Geant code simulation, the amount of the deposited energy protons in each site was calculated. Using the conversion coefficients, we converted the energy in electron volts to joules and divided it by the mass of each site to obtain the absorb dose in terms of Gy for these two sites. The results of these calculations are reported in Table 6. As can be seen in this table, the dose at the 1 micron site is different for water and organs, but at the 100 micron site, the dose is almost the same for all materials, and this table also shows that in proton therapy and in the micron dimension, the use of water instead of body organs is not recommended.

TABLE 6. The absorb dose protons at two site in water and different organs

| Energy/ site | Spleen | Thyroid | Pancreas | Prostate | Testis | Ovary | Water |
|---|---|---|---|---|---|---|---|
| 5 MeV in 100 micron site | 1.76E-04 | 1.78E-04 | 1.77E-04 | 1.76E-04 | 1.76E-04 | 1.76E-04 | 1.76E-04 |
| 1 MeV in 1 micron site | 5.41575 | 5.4793 | 5.46317 | 5.42572 | 5.4375 | 5.42746 | 5.46148 |

## Conclusions

Due to the easy access and homogeneity of water and the proximity of its adsorption properties to soft tissues as well as the proximity of water density to body organs, in most experimental and simulation studies, water instead of body organs are used. Therefore, in this research, the use of water instead of body organs in the proton therapy and its effect on stopping power, range, deposited energy, and microdosimetric spectra have been simulated and calculated. However, according to the results of this research, it was determined that in the proton therapy: Replacement of water instead of body organs in micro dimensions causes a significant error in the calculations of stopping power, range, and consequently the deposited energy in the sites. Also, this replacement (using water instead of organs) causes a maximum error of 18%, and 22% in the deposited energy in the 1 and 100 micron sites, respectively, that the amount of error depends on the energy of the incident proton. The percent difference of the proton range in water compared to the organs is constant at the high energies of the incident proton, but as we move towards the lower energy protons, this difference will increase with a relatively steep slope. Also, the use of water instead of organs has caused the displacement of the position and the intensity of the Bragg peak. It changes the microdosimetric spectra, frequency-mean lineal energy, dose-mean lineal and absorb dose. Hence this replacement causes the energy of the proton beam which is necessary to destroy the tumor not to be estimated correctly and it causes damage to surrounding healthy tissues. Therefore, for protons in the microdosimeter dimension, the use of water instead of body organs would be a significant error and thus, is not recommended. Also, using the average or the expectation value and the error propagation formula, we estimated the new formula for the statistical uncertainty of microdosimetric quantities.

## References


Ahmadi, O.L. & Tavakoli-Anbaran, H. 2015. Calculating error percentage in using water phantom instead of soft tissue concerning 103Pd brachytherapy source distribution via Monte Carlo method. *Journal of Shahid Sadoughi University of Medical Sciences* 23(9): 806-818.

Akiyama, M., Kusunoki, Y. & Umeki, S. 1992. *Radiation Research: A Twentieth-Century Perspective Volume II: Congress Proceedings*, edited by Dewey, W.C., Edington, M., Michael Fry, R.J., Hall, E.J. & Whitmore, G.F. New York: Academic Press.

Aslam, Prestwich, W.V., McNeill, F.E. & Waker, A.J. 2003. Investigating the TEPC radiation quality factor response for low energy accelerator based clinical applications. *Radiation Protection Dosimetry* 103(4): 311-322.

Blosser, T.V., Maienschein, F.C. & Freestone, R.M. 1964. The energy deposition in a water-filled spherical phantom by secondaries from high-energy protons and by neutrons. *Health Physics* 10(10): 743-750.

Bolst, D., Guatelli, S., Tran, L.T., Chartier, L., Lerch, M.L., Matsufuji, N. & Rosenfeld, A.B. 2017. Correction factors to convert microdosimetry measurements in silicon to tissue in 12C ion therapy. *Physics in Medicine & Biology* 62(6): 2055-2069.

Burigo, L., Pshenichnov, L., Mishustin, I. & Bleicher, M. 2013. Microdosimetry of radiation field from a therapeutic 12C beam in water: A study with Geant4 toolkit. *Nuclear Instruments and Methods in Physics Research Section B: Beam Interactions with Materials and Atoms* 310: 37-53.

Chattaraj, A., Selvam, T.P. & Datta, D. 2018. Investigation of applicability of pure propane gas for microdosimetry at neutron fields: A Monte Carlo study. *Radiation Protection Dosimetry* 185(1): 74-86.

Cornelius, I., Rosenfeld, A. & Bradley, P. 2002. Simulations of silicon microdosimetry measurements in fast neutron therapy. *Australasian Physical & Engineering Sciences in Medicine* 25(4): 168-171.

ICRU. 1983. *Microdosimetry. Report 36*. USA: International Commission on Radiation Units and Measurements (ICRU).

Jahanfar, S. & Tavakoli-Anbaran, H. 2019. Extracting fairly accurate proton range formulas for use in microdosimetry. *Revista Mexicana de Fisica* 65(5): 566-572.

Khan, M. & Gibbons, J.P. 2014. *Khan's the Physics of Radiation Therapy*. 5th ed. New York: Lippincott Williams & Wilkins.

Kliauga, P.J. & Rossi, H. 1982. Studies with encapsulated sources of 125I III. Microdosimetry using a non-metallic wall-less proportional counter. *International Journal of Radiation Oncology*Biology*Physics* 8(11): 1963-1968.

Lindborg, L. & Waker, A. 2017. *Microdosimetry Experimental Methods and Applications*. New York: CRC Press.

Liu, L., Prasad, S.C. & Bassano, D.A. 2003. Evaluation of two water-equivalent phantom materials for output calibration of photon and electron beams. *Medical Dosimetry* 28(4): 267-269.

Mitchell, H.H., Hamilton, T.S., Steggerda, F.R. & Bean, H.W. 1945. The chemical composition of the adult human body and its bearing on the biochemistry of growth. *Journal of Biological Chemistry* 158(3): 625-637.

Northum, J.D., Guetersloh, S.B. & Braby, L.A. 2012. FLUKA capabilities for microdosimetric analysis. *Radiation Research* 177(1): 117-123.

Pan, C.Y., Huang, Y.W., Cheng, K.H., Chao, T.C. & Tung, C.J. 2015. Microdosimetry spectra and relative biological effectiveness of 15 and 30 MeV proton beams. *Applied Radiation and Isotopes* 97: 101-105.

Rasouli, A. & Tavakoli-Anbaran, H. 2018. Estimation of the risk for the second cancers induction in healthy tissues during the radiation therapy of liver's tumor. *Iranian Journal of Radiation Safety and Measurement* 6(5): 23-30.

Rasouli, A. & Tavakoli-Anbaran, H. 2017. Study of relation between the gamma flux buildup factors and source geometry by M-C simulation. *Nuclear Science and Techniques* 28(9): 1-5.

Reniers, B., Vynckier, S. & Verhaegen, F. 2004. Theoretical analysis of microdosimetric spectra and cluster formation for 103Pd and 125I photon emitters. *Physics in Medicine & Biology* 49(16): 3781-3795.

Rosenfeld, A.B. 2016. Novel detectors for silicon based microdosimetry, their concepts and applications. *Nuclear Instruments and Methods in Physics Research Section A: Accelerators, Spectrometers, Detectors and Associated Equipment* 809: 156-170.

Rosenfeld, A.B., Bradley, P.D., Cornelius, I., Kaplan, G.I., Allen, B.J., Flanz, J.B., Goitein, M., Van Meerbeeck, A., Schubert, J., Bailey, J. & Takada, Y. 2000. A new silicon detector for microdosimetry applications in proton therapy. *IEEE Transactions on Nuclear Science* 47(4): 1386-1394.

Rossi, H.H. & Zaider, M. 2011. *Microdosimetry and Its Applications*. Berlin: Springer.

Sechopoulos, I., Rogers, D.W.O., Bazalova-Carter, M., Bolch, W.E., Heath, E.C., McNitt-Gray, M.F., Sempau, J. & Williamson, J.F. 2018. RECORDS: Improved reporting of Monte Carlo radiation transport studies: Report of the AAPM research committee task group 268. *Medical Physics* 45(1): e1-e5.

Shahrabi, M. & Tavakoli-Anbaran, H. 2015. Calculating dosimetry parameters in brachytherapy using the continuous beta spectrum of Sm-153 in the Monte Carlo simulation approach. *The European Physical Journal Plus* 130(2): 1-8.

Thomas, R.H. & Perez-Mendez, V. 1979. *Advances in Radiation Protection and Dosimetry in Medicine*. 3rd ed. New York: Springer.

Toburen, L.H. & Wilson, W.E. 1977. Energy and angular distributions of electrons ejected from water vapor by 0.3-1.5 MeV protons. *The Journal of Chemical Physics* 66(11): 5202-5213.

Tsoulfanidis, N. 2015. *Measurement and Detection of Radiation*. 4th ed. United Kingdom: Taylor & Francis.

Tsuda, S., Sato, T., Takahashi, F., Satoh, D., Endo, A., Sasaki, S., Namito, Y., Iwase, H., Ban, S. & Takada, M. 2010. Measurement of microdosimetric spectra with a wall-less tissue-equivalent proportional counter for a 290 MeV/u12C beam. *Physics in Medicine & Biology* 55(17): 5089-5101.

Ziegler, J.F. 1999. Stopping of energetic light ions in elemental matter. *Journal of Applied Physics* 85(3): 1249-1272.

Ziegler, J.F., Ziegler, M.D. & Biersack, J.P. 2008. *SRIM – the Stopping and Range of Ions in Matter*. Maryland: Library of Congress Cataloging in Publication Data.

*Corresponding author; email: tavakoli.anbaran@gmail.com